

Coherent surface acoustic wave–spin wave interactions detected by micro-focused Brillouin light scattering spectroscopy

Yannik Kunz, Matthias Küß, Michael Schneider, Moritz Geilen, Philipp Pirro, Manfred Albrecht, Mathias Weiler





Angaben zur Veröffentlichung / Publication details:

Kunz, Yannik, Matthias Küß, Michael Schneider, Moritz Geilen, Philipp Pirro, Manfred Albrecht, and Mathias Weiler. 2024. "Coherent surface acoustic wave–spin wave interactions detected by micro-focused Brillouin light scattering spectroscopy." *Applied Physics Letters* 124 (15): 152403. <https://doi.org/10.1063/5.0189324>.

RESEARCH ARTICLE | APRIL 09 2024

Coherent surface acoustic wave–spin wave interactions detected by micro-focused Brillouin light scattering spectroscopy ^{EP}

Special Collection: [Magnonics](#)


Yannik Kunz  ; Matthias Küß ; Michael Schneider ; Moritz Geilen ; Philipp Pirro ; Manfred Albrecht ; Mathias Weiler 




Appl. Phys. Lett. 124, 152403 (2024)

<https://doi.org/10.1063/5.0189324>






Lock-in Amplifier



Boxcar Averager

Boost Your Optics and Photonics Measurements

 Zurich Instruments

[Find out more](#)

Coherent surface acoustic wave–spin wave interactions detected by micro-focused Brillouin light scattering spectroscopy

Cite as: Appl. Phys. Lett. **124**, 152403 (2024); doi: [10.1063/5.0189324](https://doi.org/10.1063/5.0189324)

Submitted: 28 November 2023 · Accepted: 16 March 2024 ·

Published Online: 9 April 2024



View Online



Export Citation



CrossMark

Yannik Kunz,^{1,a)}  Matthias Küß,²  Michael Schneider,¹  Moritz Ceilen,¹  Philipp Pirro,¹  Manfred Albrecht,²  and Mathias Weiler¹ 

AFFILIATIONS

¹Fachbereich Physik and Landesforschungszentrum OPTIMAS, Rheinland-Pfälzische Technische Universität Kaiserslautern-Landau, 67663 Kaiserslautern, Germany

²Institute of Physics, University of Augsburg, 86135 Augsburg, Germany

Note: This paper is part of the APL Special Collection on Magnonics.

a) Author to whom correspondence should be addressed: ykunz@rptu.de

ABSTRACT

We investigated the interaction of surface acoustic waves and spin waves with spatial resolution by micro-focused Brillouin light scattering spectroscopy in a $\text{Co}_{40}\text{Fe}_{40}\text{B}_{20}$ (10 nm) ferromagnetic layer on a LiNbO_3 -piezoelectric substrate. We experimentally demonstrate that the magnetoelastic excitation of magnons by phonons is coherent by studying the interference of light scattered off generated magnons and annihilated phonons. We find a pronounced spatial dependence of the phonon annihilation and magnon excitation, which we map as a function of the magnetic field. The coupling efficiency of the surface acoustic waves (SAWs) and the spin waves is characterized by a magnetic field-dependent decay of the SAWs amplitude.

© 2024 Author(s). All article content, except where otherwise noted, is licensed under a Creative Commons Attribution (CC BY) license (<https://creativecommons.org/licenses/by/4.0/>). <https://doi.org/10.1063/5.0189324>

Surface Acoustic Waves (SAWs) with frequencies in the gigahertz regime have wavelengths on the micrometer scale. They, thus, enable the miniaturization of microwave components and are ubiquitous in everyday devices.^{1–3} SAW devices are further used, for instance, for probing material properties,⁴ rf signal processing,^{5,6} or sensors.⁷ Interdigital transducers (IDTs) thereby enable coherent and energy-efficient excitation and detection of SAWs on piezoelectric substrates with sufficiently small insertion losses for quantum applications.⁸ If SAWs propagate in magnetically ordered materials, the coupling of acoustic and magnetic excitations opens up a wide branch of possibilities.^{9,10} The magnetoacoustic control enables, for instance, magnetic switching,^{11,12} the creation and control of skyrmions,^{13,14} the generation of Terahertz radiation,¹⁵ magnetic field controlled phase-shifting of acoustic waves,¹⁶ acoustically driven linear and nonlinear spin wave resonance,^{17–20} and acoustic spin-charge conversion.^{21,22} The coupling of SAWs and spin waves (SWs) breaks time-reversal symmetry, and the concomitant nonreciprocal SAW transmission^{23–25} may find applications for nonreciprocal miniaturized microwave devices.^{26–28}

Commonly, the interaction between SAWs and SWs devices is studied using electrical measurement techniques by determining the magnetic

field-dependent SAW transmission from IDT to IDT as detailed, e.g., in Refs. 18 and 24. Measuring the SAW transmission allows for studying the SW dispersion and the symmetry of the magnetoacoustic interaction.²⁹ However, this electrical measurement technique does not offer spatial resolution. Previous studies used imaging techniques to resolve SAW propagation in magnetic media^{30–32} and established separate detection of SAW and SW signals.³³ While the widely used model for SAW–SW interaction¹⁷ implicitly assumes coherent SAW–SW interaction as the mechanism causing the detected SAW absorption, experimental proof for the coherency is missing. Particularly, Brillouin light scattering proved to be a versatile investigation technique to investigate magnetoacoustic resonances with spatial resolution.^{34,35} In contrast to previous studies, which utilized time-resolved detection techniques to identify coherent magnon-polarons excited by optical pumping,^{36–38} we employ excitation of SAWs by microwaves via IDTs, as commonly used in rf devices.¹ However, these works could not demonstrate the spatial dependency of the SAW–SW conversion, and the coherency of the SAW and SW remains an additional important open question as identified in Ref. 31.

Here, we use micro-focused Brillouin light scattering (μBLS) to study the magnetoacoustic interaction of SAWs with SWs on a

LiNbO₃/Co₄₀Fe₄₀B₂₀(10 nm)-structure with frequency and spatial resolution. By taking advantage of the tunable sensitivity of μ BLS to both phonons and magnons,^{34,39} we are able to separately investigate the absorption of phonons and the excitation of magnons in the system. We observe clear experimental evidence for the coherence of annihilated phonons and generated magnons by interference of the two corresponding signals, which leads to a distortion of the typical Lorentzian line shape. This results in a Fano-resonance-like line shape^{40,41} as predicted for magnetoacoustic waves by Latcham *et al.*⁴² We further reveal the spatial dependency of the phonon-magnon conversion process within the 10 nm thick Co₄₀Fe₄₀B₂₀ (CoFeB) film. A schematic depiction of the used μ BLS-setup is shown in Fig. 1(a). A more detailed description of the setup is given in the supplementary material.

In the first part of our investigation, we characterized the phonon-spectra excited by the IDT by varying the applied rf-frequency f_{MW} in the range of 2–8 GHz. The obtained BLS-spectra were integrated in BLS-frequency for each rf-frequency. The resulting phonon excitation spectrum of the IDT is shown in Fig. 1(b). Excitation peaks arise periodically at frequencies f_m fulfilling the condition of constructive interference,

$$f_n \dots \frac{c_{SAW}}{d} \quad n = 500 \text{ MHz} \quad n; \quad n = 2 \text{ f1; } 3; 5; \dots g; \quad (1)$$

where d denotes the periodicity of the IDT. In Fig. 1(b), the lowest frequency peak corresponds to the fifth harmonic order of the IDT at 2.48 GHz. The SAW excitation efficiency decreases with frequency.

This can be understood by considering that the excitation spectrum is proportional to the Fourier-transform of the electrical field generated by the IDTs.^{43,44}

To investigate the magnetic field-dependent coupling of phonons and magnons, the laser spot is positioned about 100 μ m into the ferromagnetic layer at “ROI 1,” as indicated in Fig. 1(a). We make use of the rotatable $\lambda=2$ plate, which allows for tuning the relative sensitivity of our BLS setup to magnons or phonons.³⁴ We excited the SAW at an rf-frequency of 5.45 GHz (11th order) and a microwave output power of 18 dBm. The sample was oriented so that the angle between the propagation direction of the SAW given by k_{SAW} and the external magnetic field $\mu_0 H_{ext}$ was about $\varphi = 33^\circ$. We integrated the BLS-spectra in the range of 5.25 to 5.925 GHz for both the phonon and the magnon polarization of the $\lambda=2$ plate. The resulting intensities as a function of the external magnetic field are given in Fig. 2 for (a) the phonon- and (b) the magnon signal.

First, we discuss in panel (a) the phonon signal. Here, dips in the BLS signal are observed at a positive magnetic field of $\mu_0 H_{ext} \dots 13$ mT and a negative field of $\mu_0 H_{ext} \dots -11.5$ mT. The concomitant reduction in phonon number is attributed to resonant magnon-phonon coupling at the triple crosspoint [see the inset in Fig. 2(b)] between the linear SAW dispersion relation $f_{SAW} \dots c_{SAW}k=2\pi$ (green), the SW dispersion relation (red), and the excitation frequency (gray). The magnon dispersion relation is calculated using the Kalinikos–Slavin-equation:⁴⁵

$$f_{SW} \delta k; H \dots \frac{g \mu_B \mu_0}{2\pi \hbar} H_{ext} \dots \frac{2A}{\mu_0 M_S} k^2 \dots H_{ani} \dots M_S \quad \frac{1}{j k j k j t} \quad H_{ext} \dots \frac{2A}{\mu_0 M_S} k^2 \dots H_{ani} \dots M_S \quad 1 \quad \frac{1}{j k j k j t} \sin^2 \delta \varphi \dots (2)$$

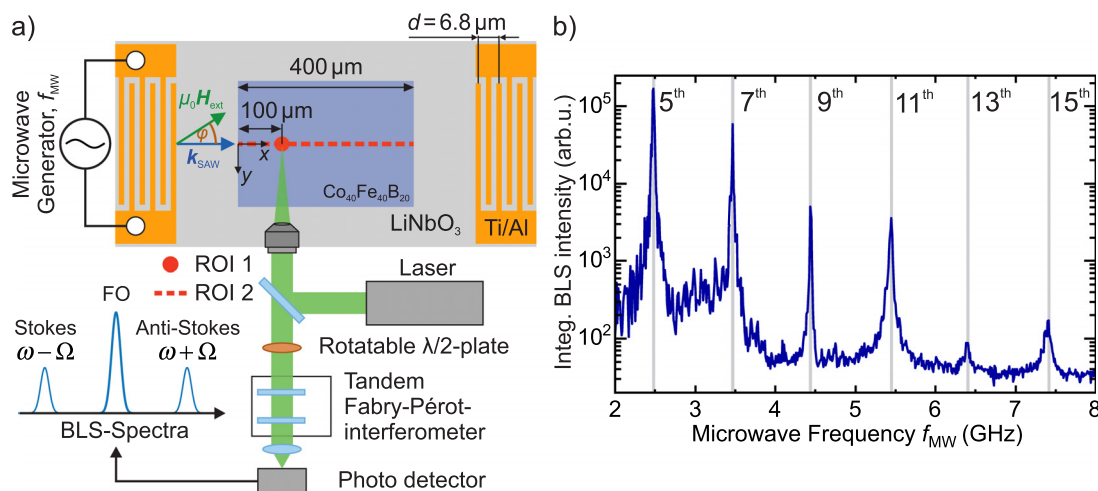


FIG. 1. (a) Schematic depiction of the used sample and the measurement configuration. On a LiNbO₃ piezoelectric substrate, a 10 nm thick and 400 μ m wide Co₄₀Fe₄₀B₂₀ layer is deposited between two sets of IDTs with a finger periodicity of 6.8 μ m and 30 finger pairs (not all shown in the figure). The external magnetic field $\mu_0 H_{ext}$ is oriented along $\varphi = 32.6^\circ$ relative to the propagation direction of the SAW k_{SAW} . We used micro-focused BLS for phonon and magnon spectroscopy, while a microscope camera allows for measuring with space resolution (not shown). The position of the laser spot during the measurements is indicated by the red dot (fixed position) and the red dashed line (linescan). The ROI 2 starts at the beginning of the ferromagnetic layer. (b) The excitation spectra of the employed set of IDTs are determined by the integration of the detected BLS intensity, measured around 10 μ m behind the IDT on the LiNbO₃. The excitation peaks arise if the condition of constructive interference for emitted SAWs between the IDT fingers is fulfilled.

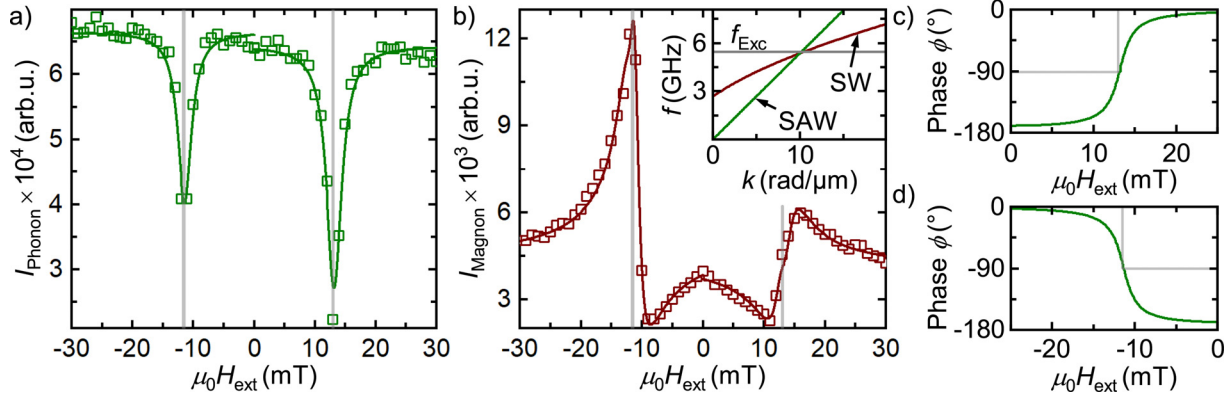


FIG. 2. (a) The integrated BLS-intensity at ROI 1 measured on phonon-polarization as a function of the external magnetic field $\mu_0 H_{\text{ext}}$. Two dips form at the positive and negative resonant magnetic field (gray lines) with different magnitudes, indicating a variation in the coupling efficiency caused by the helicity mismatch effect. Squares denote the experimental data and solid curves the fit, in panel (a) according to Eq. (4) and in panel (b) according to Eq. (9). In (b), the resulting BLS-intensity close to pure magnon-polarization is shown. The phase shift between generated magnons and annihilated phonons affects the detection via μ BLS and leads to dip-peak-like behavior. The inset in (b) shows the triple crosspoint between the excitation frequency $f_{\text{Exc}} \dots 5.45$ GHz and the dispersion relations of the SAW and the SWs at $\mu_0 H \dots 11$ mT. In (c) and (d), the phase shift ϕ between the phonons and the magnons as a function of the external magnetic field is shown.

We used broadband ferromagnetic resonance spectroscopy (see the supplementary material) to determine the g-factor $g \dots 2.1108$, Gilbert damping parameter $\alpha \dots 0.00607$, saturation magnetization $\mu_0 M_S \dots 1.287$ T, and anisotropy field $\mu_0 H_{\text{ani}} \dots 1.46$ mT of our CoFeB film. The small field shift between the positive and negative resonance magnetic field is attributed to an offset of the Hall probe rather than any SW nonreciprocity. The different dip intensities for positive and negative magnetic fields are attributed to the helicity mismatch effect.^{23,24} When changing directions of the magnetic field, the helicity of the spin wave is inverted, while the helicity of the SAW remains the same, as it is determined by the SAWs propagation direction. The helicity mismatch effect gives rise to different coupling efficiencies on whether the helicities match (pos. field) or mismatch (neg. field), thus leading to different dip magnitudes.¹⁰

We model the obtained phonon signal as follows. Following Ref. 46, we assume that the obtained phonon BLS intensity is proportional to the out-of-plane displacement u_z^2 ,

$$I_{\text{Ph}}(\delta x; H) \propto \int_0^{\delta x} \int_0^{\delta x} u_z^2(\delta x; t; H) dt dk; \quad (3)$$

The displacement after a certain propagation distance x becomes magnetic field dependent due to the absorption of SAW phonons by SW generation. We derive the absorption of SAW power by following the approach of Küß *et al.*²⁴ and make use of the correlation between the SAW power and the displacement $P_{\text{SAW}} \propto u_z^2$. Thus, the expected BLS intensity can be written as

$$I_{\text{Ph}}(\delta x; H) \dots I_0 \exp \delta C_1 \text{Im} \delta \chi_{11} \delta H \delta x; \quad (4)$$

where I_0 is the BLS intensity obtained from the SAW at the launching IDT, C_1 is a constant that quantifies the SAW-SW conversion efficiency, and $\chi_{11} \delta H$ is the diagonal component of the magnetic susceptibility tensor χ . In this simple model, the SAW-SW helicity mismatch effect is phenomenologically taken into account by using different C_1 for $\mu_0 H_{\text{ext}} < 0$ and $\mu_0 H_{\text{ext}} > 0$. The helicity mismatch effect leads to

different magnitudes of the SAW-SW-resonance in Fig. 2(a), which, in turn, characterizes the nonreciprocal coupling.^{23,24} We derive χ by solving the Landau-Lifshitz-Gilbert-equation (see the supplementary material) and fit Eq. (4) to the data in Fig. 2(a), with fitting parameters I_0 and C_1 . Generally, the coupling parameters C_1 and C_2 depend on the direction ϕ of the applied external magnetic field, as the components of the magnetoacoustic driving field depend on the propagation direction of the SAW. As can be seen in Fig. 2(a), good agreement between the BLS-intensity and the fitting model can be obtained.

Next, we consider the obtained BLS signal measured at optimized magnon detection efficiency by rotating the $\lambda=2$ plate correspondingly. Since the number of phonons is always significantly higher than the number of newly excited magnons, the fraction of the unfiltered phonon signal cannot be neglected and has to be taken into account. We observe a peak-dip-like behavior, as can be seen in Fig. 2(b), which we explain as follows: on resonance, phonons are annihilated, and magnons are generated. Because of the coherency of this process, the photons inelastically scattering off these magnons, and phonons can interfere with each other. When sweeping through the resonance field, the phase relation between magnons and phonons changes, as detailed later, so that the interference is destructive/constructive depending on the magnetic field. This leads to a Fano-resonance-like line shape.⁴⁰ To describe the obtained signal, we start by writing the BLS intensity as

$$I_{\text{Ma}}(\delta x; H) \propto \int_0^{\delta x} \int_0^{\delta x} \delta c_{\text{Ph}} u_z \delta x; t; H \delta c_{\text{Ma}} m_z \delta x; t; H \delta x^2 dt dk; \quad (5)$$

with c_{Ph} and c_{Ma} representing the detection efficiency of the phononic and the magnonic signal at the given position of the $\lambda=2$ plate, m_z the dynamic out-of-plane magnetization component of the SW, and u_z the displacement due to the SAW. For the dynamic magnetization component m_z and the displacement u_z , we make the generalized wave-like Ansatz

$$u_z \delta x; t; H \dots u_{z,0} \delta x; H \exp \delta i \delta \omega t - k x \delta x; \quad (6)$$

$$m_z \delta x; t; H \delta \dots m_{z,0} \delta x; H \delta \exp \delta i \delta \omega t - k x \delta \phi \delta H \delta \delta \delta; \quad (7)$$

where $u_{z,0} \delta x; H \delta$ and $m_{z,0} \delta x; H \delta$ are the magnetic field and spatially dependent amplitudes of the displacement and the dynamic magnetization, respectively. We also include the phase shift $\phi \delta H \delta$ between the SAW driven dynamic magnetization and the SAW itself, similar to the classical driven harmonic oscillator, where a phase shift of $\phi \dots 90^\circ$ is expected at resonance. The displacement u_z can be derived as previously from the SAW power in Eq. (4).

The magnetic component m_z is derived by the locally absorbed SAW power as due to the high Gilbert damping in the system, only the locally excited magnons contribute to the BLS signal, as will be discussed in more detail later on. By assuming that the SW power is proportional to the dynamic out-of-plane magnetization component P_{SW} / m_z^2 and the locally absorbed SAW power $P_{abs,loc}$ flows into the spin wave system, we obtain

$$m_z \delta x; H \delta / P_{abs,loc} \propto \text{Im} \delta \chi_{11} \delta h_{dr} \delta x; H \delta; \quad (8)$$

with the driving field h_{dr} generated by the SAW. As the amplitude of the SAW decreases with increasing propagation length, so does the driving field. In turn, the driving field h_{dr} can again be derived using the displacement u_z by h_{dr} / u_z . Thus, we obtain for the expected BLS intensity by only taking the real part of Eq. (5) and neglecting higher order terms that are not linear in c_{ph} ,

$$I_{Ma} \delta x; H \delta \dots c_{Ma}^2 C_2 \text{Im} \delta \chi_{11} \delta \exp \delta - C_1 \text{Im} \delta \chi_{11} \delta x \delta \propto \frac{1}{P_{abs,loc}} \text{Im} \delta \chi_{11} \delta \exp \delta - C_3 \text{Im} \delta \chi_{11} \delta x \delta \cos \delta \phi \delta; \quad (9)$$

Here, C_2 and C_3 are again constant prefactors included for simplification and to combine other constant prefactors. We use Eq. (9) to fit the data in Fig. 2(b). As can be seen, we achieve good agreement between the obtained experimental data and our model. In Figs. 2(c) and 2(d), the resulting phase shift between the SAW and the SW is shown, becoming 90° at the resonant coupling field in agreement with the expectation for a driven harmonic oscillator. We note that describing the obtained BLS-signals in Fig. 2(b) by a simple superposition of the phononic and the magnonic signals is not sufficient. By

taking the interfering BLS-signals of the two quasi-particles into account, we obtain a suitable description of the measured data. We, thus, conclude that a coherent phonon-to-magnon conversion is present in our experiment. Hence, our experimental data provide evidence for a well-defined phase relation and consequently coherency between the annihilated phonons and generated magnons.

Next, we map the magnetoelastic coupling as a function of the external magnetic field and the propagation distance of the SAW. For this, we use an excitation frequency of 2.48 GHz at an excitation power of 18 dBm and exploit the second-order harmonic generation^{32,47,48} of the tenth order IDT resonance at 5 GHz to investigate the space-dependent coupling. The magnetic field was aligned as before ($\phi = 32.6^\circ$); however, now a linescan measurement was performed, as indicated by the red dashed line labeled “ROI 2” in Fig. 1(a). Again, we measured using both phonon and magnon polarization and integrated the resulting BLS-spectra in BLS-frequency. The results are presented in Fig. 3, in panel (a), for the obtained phonon signal and in (b), the magnon signal, as a function of the applied magnetic field $\mu_0 H_{ext}$ and the propagation length x . Here, the scaled intensity on phonon-polarization at 30 mT is subtracted in order to remove the unfiltered phononic signal.

First, we discuss the obtained phonon signal. Here, two dips of different magnitudes start to form with increasing propagation length x over the ferromagnetic layer. The magnetic fields at which the dips occur again correspond to the triple crosspoint between the excitation frequency and the dispersion relations of the SAW and the SW, as discussed before. The magnetic field dependence of the phonon signal becomes more pronounced with increased SAW propagation because of the progressive SAW absorption during its propagation in the CoFeB film. This finding supports the previously observed dependence of the electrically detected magnetoelastic interaction on the length of the magnetic film.²⁵

We now turn to the magnon signal shown in Fig. 3(b), where the highest excitation of magnons is found at the beginning of the ferromagnetic layer. Due to the considerably large Gilbert damping α in the CoFeB film, magnons have a very low lifetime, leading to a short decay length $\xi_{SW} \approx 1.81 \mu\text{m}$ at $f \dots 5 \text{ GHz}$ and $\mu_0 H \dots 10$

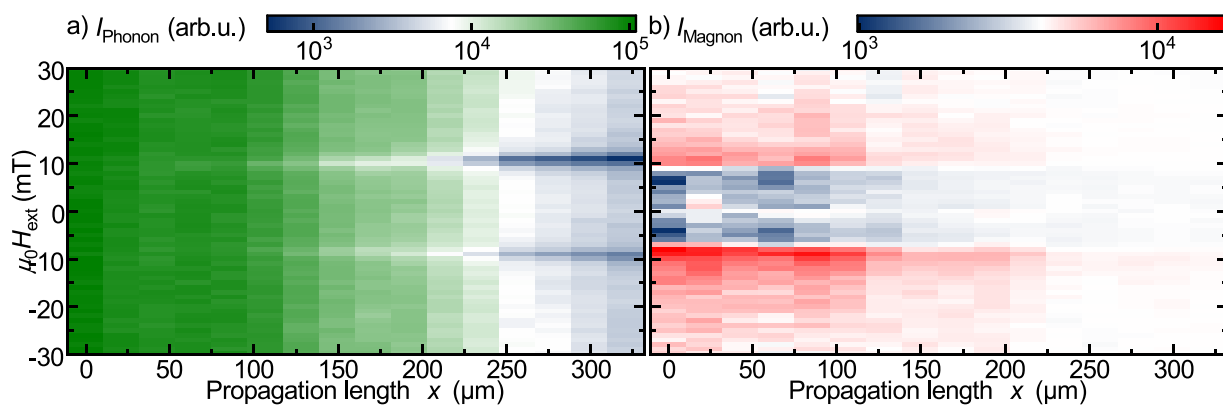


FIG. 3. Integrated BLS-intensity of the linescan measurement indicated by ROI 2 in Fig. 1(a), as a function of the external magnetic field and the propagation length of the SAW. We evaluated the excitation of the tenth harmonic order at a frequency of 5 GHz, which is excited by nonlinear phonon processes in the LiNbO₃. In (a), the measured intensity on phonon-polarization is shown, where it can be seen that with increasing propagation length, two dips form at the resonant magnetic field. (b) The obtained intensity on magnon polarization (the scaled intensity on phonon-polarization at 30 mT is subtracted). The highest increase in magnon population occurs at the start of the ferromagnetic layer at resonant magnetic field and decreases with vanishing phonon amplitude.

mT in Damon–Eshbach geometry (see the supplementary material), thus vanishing almost instantly. Consequently, the magnon population does not build up with increasing propagation length, and only locally excited SWs by the SAW are detected. Since the phonon density is highest at the start of the ferromagnetic layer, the highest excitation of magnons is found here, while fewer magnons are excited with increasing propagation length. The coupling of the phonon to the magnon system opens a loss channel for the propagating SAW phonons. From the previously obtained data, we now determine the magnetic field dependency of the SAW amplitude decay rate. We obtain an exponential decrease in SAW amplitude with propagation distance, which is characterized by the effective damping parameter $\eta_{\text{eff}} \delta H \delta$, which we derive from the BLS-intensity by fitting

$$I_{\text{Phonon}} \propto x; H \delta \dots I_{0, \text{Phonon}} \exp \delta 2 \eta_{\text{eff}} \delta H \delta x \delta \quad (10)$$

The factor 2 results from the fact that the BLS intensity is proportional to the SAW intensity, which is again proportional to the squared SAW amplitude. We determine the effective damping by plotting the BLS-intensity as a function of the propagation length x for each magnetic field in logarithmic representation as illustrated in Fig. 4. The obtained effective damping rates η_{eff} are shown in Fig. 5. The decay rate increases at the resonant coupling field with different magnitudes, indicating a nonreciprocal SAW-SW coupling,¹⁰ by 74% at 11 mT and 41% at 9 mT in comparison to off-resonant fields.

In summary, we demonstrated spatially resolved coherent interaction between phonons and magnons by micro-focused Brillouin light scattering experiments. By exploiting the shift in polarization of light scattered by magnons, we selectively detected the excitation of magnons and the absorption of phonons as a function of the applied magnetic field. We found that magnonic and phononic BLS-signals interfere, which demonstrates the coherence in the phonon-to-magnon conversion process. By taking the coherent phase relation between SAW and SW into consideration, we formulated a phenomenological model for the expected BLS intensity, which we used to fit our data. Phonon excitation via IDTs revealed coherency of the phonon-to-magnon conversion even in the absence of an identification of the avoided crossing of the dispersion relation of the two quasiparticles. Our spatially resolved data show that the SAW-SW

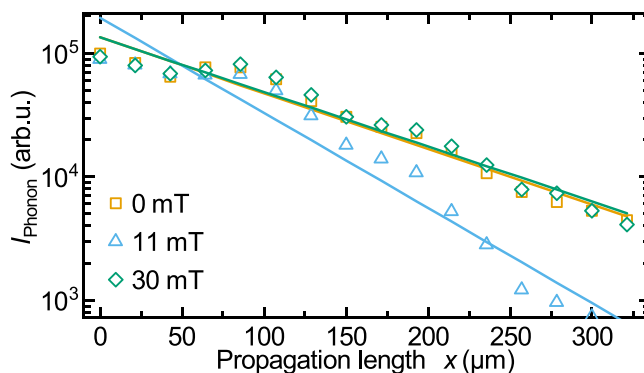


FIG. 4. Decrease of the SAW amplitude with propagation length, shown for different magnetic fields at a SAW frequency of 5 GHz. At 11 mT (resonant magnetic coupling field), the decrease in SAW amplitude is enhanced compared to off-resonant magnetic fields.

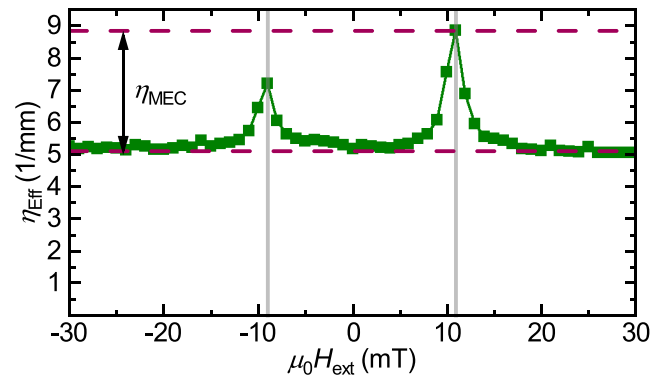


FIG. 5. Increase of the phonon decay rate due to the magnetoelastic coupling with SW at 5 GHz as a function of the external magnetic field. The different magnitudes in peaks are denoted to the helicity mismatch effect that results in a nonreciprocal SAW transmission.

interaction does not result in increased SW propagation length.³¹ This finding and the interference of phonons and magnons need to be considered for potential applications that rely on magnetoacoustically generated magnons or magnon-controlled phonon propagation.

See the supplementary material for details regarding the phenomenological modeling of the magnetoacoustic interaction, the used μ BLS-setup by the sample fabrication, and the characterization of magnetic properties using broadband ferromagnetic resonance spectroscopy.

This work was funded by the Deutsche Forschungsgemeinschaft (DFG, German Research Foundation)—Project No. 492421737, the DFG TRR 173—268565370 (project B01), and by the European Union within the HORIZON-CL4-2021-DIGITAL-EMERGING-01 under Grant No. 101070536 M&MEMS.

AUTHOR DECLARATIONS

Conflict of Interest

The authors have no conflicts to disclose.

Author Contributions

Yannik Kunz: Data curation (lead); Formal analysis (lead); Investigation (lead); Methodology (equal); Visualization (lead); Writing – original draft (equal). **Matthias Küß:** Conceptualization (lead); Formal analysis (supporting); Methodology (equal); Resources (equal); Writing – review & editing (equal). **Michael Schneider:** Formal analysis (equal); Investigation (equal); Methodology (equal); Supervision (lead). **Moritz Geilen:** Formal analysis (equal); Investigation (equal); Methodology (equal); Supervision (supporting); Writing – review & editing (supporting). **Philipp Pirro:** Funding acquisition (supporting); Project administration (supporting); Resources (supporting); Writing – review & editing (equal). **Manfred Albrecht:** Funding acquisition (equal); Project administration (supporting); Resources (supporting); Writing – review & editing (supporting). **Mathias Weiler:** Conceptualization (supporting); Formal analysis

(supporting); Funding acquisition (equal); Investigation (supporting); Methodology (supporting); Project administration (lead); Resources (supporting); Supervision (lead); Visualization (supporting); Writing – review & editing (equal).

DATA AVAILABILITY

The data that support the findings of this study are available from the corresponding author upon reasonable request.

REFERENCES

- ¹C. K. Campbell, *Surface Acoustic Wave Devices for Mobile and Wireless Communications* (Applications of Modern Acoustics, Academic Press, San Diego, CA, 1998).
- ²K. Länge, B. E. Rapp, and M. Rapp, “Surface acoustic wave biosensors: A review,” *Anal. Bioanal. Chem.* **391**, 1509 (2008).
- ³T. Franke, A. R. Abate, D. A. Weitz, and A. Wixforth, “Surface acoustic wave (SAW) directed droplet flow in microfluidics for PDMS devices,” *Lab Chip* **9**, 2625 (2009).
- ⁴A. M. Lomonosov and P. Hess, “Impulsive fracture of silicon by elastic surface pulses with shocks,” *Phys. Rev. Lett.* **89**, 095501 (2002).
- ⁵I. A. Viktorov, *Rayleigh and Lamb Waves: Physical Theory and Applications* (Springer/Plenum Press, New York, NY, 1967).
- ⁶K.-Y. Hashimoto, *Surface Acoustic Wave Devices in Telecommunications: Modeling and Simulation* (Springer-Verlag, Berlin, Heidelberg, 2000).
- ⁷B. Paschke, A. Wixforth, D. Denysenko, and D. Volkmer, “Fast surface acoustic wave-based sensors to investigate the kinetics of gas uptake in ultra-microporous frameworks,” *ACS Sens.* **2**, 740 (2017).
- ⁸M. K. Ekström, T. Aref, J. Runeson, J. Björck, I. Boström, and P. Delsing, “Surface acoustic wave unidirectional transducers for quantum applications,” *Appl. Phys. Lett.* **110**, 073105 (2017).
- ⁹W.-G. Yang and H. Schmidt, “Acoustic control of magnetism toward energy-efficient applications,” *Appl. Phys. Rev.* **8**, 021304 (2021).
- ¹⁰M. Küß, M. Albrecht, and M. Weiler, “Chiral magnetoacoustics,” *Front. Phys.* **10**, 981257 (2022).
- ¹¹W. Li, B. Buford, A. Jander, and P. Dhagat, “Writing magnetic patterns with surface acoustic waves,” *J. Appl. Phys.* **115**, 17E307 (2014).
- ¹²L. Thevenard, I. S. Camara, S. Majrab, M. Bernard, P. Rovillain, A. Lemaître, C. Gourdon, and J.-Y. Duquesne, “Precessional magnetization switching by a surface acoustic wave,” *Phys. Rev. B* **93**, 134430 (2016).
- ¹³Y. Tomoyuki, S. Satoshi, R. Bivas, S. Shinichiro, O. Naoki, K. Shinya, and O. Yoshichika, “Creation of magnetic skyrmions by surface acoustic waves,” *Nat. Nanotechnol.* **15**, 361–366 (2020).
- ¹⁴R. Chen, C. Chen, L. Han, P. Liu, R. Su, W. Zhu, Y. Zhou, F. Pan, and C. Song, “Ordered creation and motion of skyrmions with surface acoustic wave,” *Nat. Commun.* **14**, 4427 (2023).
- ¹⁵W. Zhang, P. Maldonado, Z. Jin, T. Seifert, J. Arabski, G. Schmerber, E. Beaurepaire, M. Bonn, T. Kampfrath, P. M. Oppeneer, and D. Turchinovich, “Ultrafast terahertz magnetometry,” *Nat. Commun.* **11**, 4247 (2020).
- ¹⁶P. Rovillain, J. Y. Duquesne, L. Christienne, M. Eddrief, M. G. Pini, A. Rettori, S. Tacchi, and M. Marangolo, “Impact of spin-wave dispersion on surface-acoustic-wave velocity,” *Phys. Rev. Appl.* **18**, 064043 (2022).
- ¹⁷L. Dreher, M. Weiler, M. Pernpeintner, H. Huebl, R. Gross, M. Brandt, and S. Goennenwein, “Surface acoustic wave-driven ferromagnetic resonance in nickel thin films: Theory and experiment,” *Phys. Rev. B* **86**, 134415 (2012).
- ¹⁸M. Weiler, L. Dreher, C. Heeg, H. Huebl, R. Gross, M. S. Brandt, and S. T. B. Goennenwein, “Elastically driven ferromagnetic resonance in nickel thin films,” *Phys. Rev. Lett.* **106**, 117601 (2011).
- ¹⁹M. Geilen, R. Verba, A. Nicoloiu, D. Narducci, A. Dinescu, M. Ender, M. Mohseni, F. Ciubotaru, M. Weiler, A. Müller, B. Hillebrands, C. Adelman, and P. Pirro, “Parametric excitation and instabilities of spin waves driven by surface acoustic waves,” *arXiv:2201.04033* (2022).
- ²⁰P. J. Shah, D. A. Bas, A. Hamadeh, M. Wolf, A. Franson, M. Newburger, P. Pirro, M. Weiler, and M. R. Page, “Symmetry and nonlinearity of spin wave resonance excited by focused surface acoustic waves,” *Adv. Electron. Mater.* **9**, 2300524 (2023).
- ²¹M. Weiler, H. Huebl, F. S. Goerg, F. D. Czeschka, R. Gross, and S. T. B. Goennenwein, “Spin pumping with coherent elastic waves,” *Phys. Rev. Lett.* **108**, 176601 (2012).
- ²²T. Kawada, M. Kawaguchi, T. Funato, H. Kohno, and M. Hayashi, “Acoustic spin Hall effect in strong spin-orbit materials,” *Sci. Adv.* **7**, eabd9697 (2021).
- ²³M. Xu, K. Yamamoto, J. Puebla, K. Baumgaertl, B. Rana, M. Miura, H. Takahashi, D. Grundler, S. Maekawa, and Y. Otani, “Nonreciprocal surface acoustic wave propagation via magneto-rotation coupling,” *Sci. Adv.* **6**, eabb1724 (2020).
- ²⁴M. Küß, M. Heigl, L. Flacke, A. Hörner, M. Weiler, M. Albrecht, and A. Wixforth, “Nonreciprocal Dzyaloshinskii-Moriya magnetoacoustic waves,” *Phys. Rev. Lett.* **125**, 217203 (2020).
- ²⁵M. Küß, S. Glamsch, Y. Kunz, A. Hörner, M. Weiler, and M. Albrecht, “Giant surface acoustic wave nonreciprocity with low magnetoacoustic insertion loss in CoFeB/Ru/CoFeB synthetic antiferromagnets,” *ACS Appl. Electron. Mater.* **5**, 5103–5110 (2023).
- ²⁶R. Verba, I. Lisenkov, I. Krivorotov, V. Tiberkevich, and A. Slavin, “Nonreciprocal surface acoustic waves in multilayers with magnetoelastic and interfacial Dzyaloshinskii-Moriya interactions,” *Phys. Rev. Appl.* **9**, 064014 (2018).
- ²⁷B. Liang, B. Yuan, and J.-C. Cheng, “Acoustic diode: Rectification of acoustic energy flux in one-dimensional systems,” *Phys. Rev. Lett.* **103**, 104301 (2009).
- ²⁸R. Verba, E. N. Bankowski, T. J. Meitzler, V. Tiberkevich, and A. Slavin, “Phase nonreciprocity of microwave-frequency surface acoustic waves in hybrid heterostructures with magnetoelastic coupling,” *Adv. Electron. Mater.* **7**, 2100263 (2021).
- ²⁹M. Küß, M. Heigl, L. Flacke, A. Hefe, A. Hörner, M. Weiler, M. Albrecht, and A. Wixforth, “Symmetry of the magnetoelastic interaction of Rayleigh and shear horizontal magnetoacoustic waves in nickel thin films on LiTaO₃,” *Phys. Rev. Appl.* **15**, 034046 (2021).
- ³⁰C. Zhao, Z. Zhang, Y. Li, W. Zhang, J. E. Pearson, R. Divan, Q. Liu, V. Novosad, J. Wang, and A. Hoffmann, “Direct imaging of resonant phonon-magnon coupling,” *Phys. Rev. Appl.* **15**, 014052 (2021).
- ³¹B. Casals, N. Statuto, M. Foerster, A. Hernández-Mínguez, R. Cichelero, P. Manshausen, A. Mandziak, L. Aballe, J. M. Hernández, and F. Macià, “Generation and imaging of magnetoacoustic waves over millimeter distances,” *Phys. Rev. Lett.* **124**, 137202 (2020).
- ³²M. Kraimia, P. Kuzewski, J.-Y. Duquesne, A. Lemaître, F. Margailan, C. Gourdon, and L. Thevenard, “Time- and space-resolved nonlinear magnetoacoustic dynamics,” *Phys. Rev. B* **101**, 144425 (2020).
- ³³M. G. Cottam and D. J. Lockwood, *Light Scattering in Magnetic Solids* (Wiley, 1986).
- ³⁴M. Geilen, A. Nicoloiu, D. Narducci, M. Mohseni, M. Bechberger, M. Ender, F. Ciubotaru, B. Hillebrands, A. Müller, C. Adelman, and P. Pirro, “Fully resonant magneto-elastic spin-wave excitation by surface acoustic waves under conservation of energy and linear momentum,” *Appl. Phys. Lett.* **120**, 242404 (2022).
- ³⁵A. N. Litvinenko, A. V. Sadovnikov, V. V. Tikhonov, and S. A. Nikitov, “Brillouin light scattering spectroscopy of magneto-acoustic resonances in a thin-film garnet resonator,” *IEEE Magn. Lett.* **6**, 1–4 (2015).
- ³⁶C. Berk, M. Jariš, W. Yang, S. Dhuey, S. Cabrini, and H. Schmidt, “Strongly coupled magnon-phonon dynamics in a single nanomagnet,” *Nat. Commun.* **10**, 2652 (2019).
- ³⁷F. Godejohann, A. V. Scherbakov, S. M. Kukhtaruk, A. N. Poddubny, D. D. Yaremkevich, M. Wang, A. Nadzeyka, D. R. Yakovlev, A. W. Rushforth, A. V. Akimov, and M. Bayer, “Magnon polaron formed by selectively coupled coherent magnon and phonon modes of a surface patterned ferromagnet,” *Phys. Rev. B* **102**, 144438 (2020).
- ³⁸T. Hioki, Y. Hashimoto, and E. Saitoh, “Coherent oscillation between phonons and magnons,” *Commun. Phys.* **5**, 115 (2022).
- ³⁹F. Kargar and A. A. Balandin, “Advances in brillouin-mandelstam light-scattering spectroscopy,” *Nat. Photonics* **15**, 720–731 (2021).
- ⁴⁰U. Fano, “Effects of configuration interaction on intensities and phase shifts,” *Phys. Rev.* **124**, 1866–1878 (1961).

- ⁴¹Y. S. Joe, A. M. Satanin, and C. S. Kim, "Classical analogy of Fano resonances," *Phys. Scr.* **74**, 259 (2006).
- ⁴²O. S. Latcham, Y. I. Gusieva, A. V. Shytov, O. Y. Gorobets, and V. V. Kruglyak, "Controlling acoustic waves using magneto-elastic Fano resonances," *Appl. Phys. Lett.* **115**, 082403 (2019).
- ⁴³D. Royer, S. Lyle, and E. Dieulesaint, "Elastic waves in solids II: Generation," *Acousto-optic Interaction, Applications, Advanced Texts in Physics* (Springer Berlin Heidelberg, 1999).
- ⁴⁴S. Datta, *Surface Acoustic Wave Devices* (Prentice-Hall, 1986).
- ⁴⁵B. A. Kalinikos and A. N. Slavin, "Theory of dipole-exchange spin wave spectrum for ferromagnetic films with mixed exchange boundary conditions," *J. Phys. C* **19**, 7013 (1986).
- ⁴⁶M. Cardona and G. Güntherodt, *Light Scattering in Solids III: Recent Results* (Springer-Verlag, Berlin, Heidelberg, 1982), Vol. 8.
- ⁴⁷E. G. Lean, C. C. Tseng, and C. G. Powell, "Optical probing of acoustic surface-wave harmonic generation," *J. Appl. Phys.* **16**, 32 (1970).
- ⁴⁸E. G. Lean and C. C. Tseng, "Nonlinear effects in surface acoustic waves," *J. Appl. Phys.* **41**, 3912 (1970).